SOURCE DATA TRANSPARENT PROCESS OPEN ACCESS

A role for septin 2 in Drp1-mediated mitochondrial fission

Alessandro Pagliuso[1,2,3], To Nam Tham[1,2,3,†], Julia K Stevens[4,†], Thibault Lagache[5,6], Roger Persson[7], Audrey Salles[8], Jean-Christophe Olivo-Marin[5,6], Stéphane Oddos[7], Anne Spang[4], Pascale Cossart[1,2,3,**] & Fabrizia Stavru[1,2,3,*]

Abstract

Mitochondria are essential eukaryotic organelles often forming intricate networks. The overall network morphology is determined by mitochondrial fusion and fission. Among the multiple mechanisms that appear to regulate mitochondrial fission, the ER and actin have recently been shown to play an important role by mediating mitochondrial constriction and promoting the action of a key fission factor, the dynamin-like protein Drp1. Here, we report that the cytoskeletal component septin 2 is involved in Drp1-dependent mitochondrial fission in mammalian cells. Septin 2 localizes to a subset of mitochondrial constrictions and directly binds Drp1, as shown by immunoprecipitation of the endogenous proteins and by pulldown assays with recombinant proteins. Depletion of septin 2 reduces Drp1 recruitment to mitochondria and results in hyperfused mitochondria and delayed FCCP-induced fission. Strikingly, septin depletion also affects mitochondrial morphology in *Caenorhabditis elegans*, strongly suggesting that the role of septins in mitochondrial dynamics is evolutionarily conserved.

Introduction

Mitochondria are highly dynamic eukaryotic organelles, which form an interconnected and dynamic network. Mitochondrial morphology and function are tightly interrelated. The dynamic behavior of mitochondria relies partly on their movement along cytoskeletal tracks, including microtubules, intermediate filaments, and actin (reviewed in [1]). In addition, mitochondrial network dynamics is determined by mitochondrial fusion and fission, to which the cytoskeleton also contributes. The molecular basis of mitochondrial dynamics is intensely studied from both the medical and the fundamental cell biology standpoints, as defects in this process can lead to mitochondrial dysfunction and to pathology [2–5]. The canonical mitochondrial fission mechanism involves the dynamin-like protein Drp1, which is recruited from the cytosol to mitochondria, where it oligomerizes to form spirals that constrict the mitochondrion [6]. Drp1 recruitment and oligomerization are highly regulated at the molecular level through posttranslational modifications of Drp1 (reviewed in [7]) and through the presence of several Drp1 receptors on the mitochondrial outer membrane [8–14]. Drp1-mediated fission is facilitated by ER tubules that wrap around mitochondria and constrict them. An ER-localized formin, inverted formin 2 (INF2) [15], and a mitochondria-localized Spire1 isoform (Spire1C) [16] cooperate to induce localized actin polymerization at the constriction sites [16]. In addition to this, several actin-binding proteins have been reported to participate in mitochondrial fission [17,18]. The motor protein myosin 2 (Myo2), proposed to provide actin with the necessary contractile force for mitochondrial fission ("mitokinesis" [18]), is known to not only interact with actin, but also with septins [19]. Septins are conserved eukaryotic GTP-binding proteins that are considered components of the cytoskeleton as they can form non-polar filaments (reviewed in [20,21]). Septins are highly expressed in interphase cells [22], suggesting that they play a role beyond their well-established contribution to cytokinesis [23,24]. Indeed, recent studies indicate that septins are involved in a number of different cellular processes, such as ciliogenesis [25,26], axon guidance [27], and phagocytosis, [28] and serve to restrict bacterial actin-based motility [29] and protein diffusion at the cell cortex [30], at the yeast bud neck [31], and at the ER [32]. Knockout

1 Unité des Interactions Bactéries-Cellules, Institut Pasteur, Paris, France
2 U604 Inserm, Paris, France
3 USC2020 INRA, Paris, France
4 Biozentrum, University of Basel, Basel, Switzerland
5 Unité d'Analyse d'Images Biologiques, Institut Pasteur, Paris, France
6 CNRS UMR 3691, Paris, France
7 Bioaxial, Paris, France
8 Imagopole, Citech, Institut Pasteur, Paris, France
*Corresponding author. Tel: +33 1 40613782; E-mail: fabrizia.stavru@pasteur.fr
**Corresponding author. Tel: +33 1 40613032; Fax: +33 1 45688706; E-mail: pcossart@pasteur.fr
†These authors contributed equally to this work

of any of the 13 mammalian septins leads to highly diverse pheno-types, further indicating that different septins may perform different functions [21]. Mammalian septins are subdivided into 4 groups (septin 2, septin 3, septin 6, septin 7) and form heteropolymeric complexes with the ubiquitous septin 2 (Sept2) at the heart of the complexes [20]. Septins display a complex localization pattern: Long fibers occur under the nucleus and along actin stress fibers, while both long and short fibers are found throughout the cell, accu-mulating at the cell periphery in association with actin (reviewed in [20]). Furthermore, ringlike structures decorate the cytosol and subcortical regions [33].

In contrast to actin filaments and microtubules, septins are not known to interact extensively with mitochondria. To our knowl-edge, a single report indicated that septins colocalize with mitochon-dria in the ciliate *Tetrahymena thermophila* and septin depletion/overexpression grossly disrupted mitochondrial morphology in this organism [34]. Nevertheless, the mechanism through which ciliate septins act in mitochondrial dynamics has remained elusive. Concerning mammalian septins, knockout of the differentially expressed septin 4 (Sept4) in mice has been shown to result in sperm defects, including aberrant annulus and mitochondrial archi-tecture [35]. Two Sept4 splice isoforms have furthermore been found to localize to mitochondria and participate in apoptosis and neuronal development, respectively [36,37]. To date, it is unclear whether any of the ubiquitously expressed septins is involved in mitochondrial dynamics of metazoan cells.

Here, we show that in mammalian cells Sept2 directly interacts with the mitochondrial fission protein Drp1 and is required for effi-cient localization of Drp1 at mitochondria, thus introducing septins as new players in mitochondrial dynamics.

Results

Sept2 depletion induces mitochondrial elongation

We assessed the role of septins in mitochondrial dynamics by silenc-ing three members of the family (i.e., Sept2, Sept7, and Sept9) and analyzing mitochondrial morphology through indirect immunofluo-rescence (Fig 1A). Mitochondria were significantly elongated in Sept2- and Sept7-silenced cells compared to control cells, respectively,

by 1.8-fold and 1.4-fold. In contrast, mitochondrial length did not significantly increase in Sept9-depleted cells (Fig 1B). Previous stud-ies have shown that depletion of Sept7 codepletes Sept2 [33,38,39], which could explain why depletion of either Sept2 or Sept7 causes an increase in mitochondrial length. We therefore assessed the levels of Sept2 upon Sept2, Sept7, and Sept9 depletion. In our hands, the depletion efficiency of Sept2 reached almost 90%, while that of Sept7 reached 80% and resulted in a concomitant 65% decrease in Sept2 levels, in agreement with previous reports [33,38,39]. In contrast our very efficient Sept9 depletion (97%) did not significantly co-down-regulate Sept2 (Fig EV1A–D). These findings are consistent with our observation that the depletion of Sept2 and Sept7, but not that of Sept9, affects mitochondrial length.

Given the strong mitochondrial phenotype obtained upon Sept2 depletion, we decided to focus our attention on Sept2 and its possi-ble involvement in mitochondrial dynamics. To ensure that the observed mitochondrial elongation in Sept2-depleted cells is not due to an off-target effect, we confirmed the phenotype with different Sept2-targeting siRNA sequences (Fig EV1E and F) and in different cell types (HeLa, Fig 1A; and U2OS, Fig 2D). Furthermore, the mito-chondrial elongation phenotype of Sept2-silenced cells could be rescued through overexpression of siRNA-resistant Sept2 (Fig 1C and D). Interestingly, Sept7 overexpression could also rescue the mitochondrial elongation phenotype induced by Sept2 siRNA, albeit less efficiently compared to the Sept2 siRNA-resistant construct, that is, 54% rescue upon Sept7 overexpression compared to 70% rescue for the overexpression of siRNA-resistant Sept2 (Fig 1D). These results further suggest that both proteins play a role in mitochon-drial dynamics (see Discussion).

We next asked whether increasing the amount of Sept2 would induce mitochondrial fission. Similar to Drp1 overexpression [40], overexpression of HA-tagged Sept2 did not substantially induce mitochondrial fragmentation (our unpublished results), consistent with the notion that mitochondrial fission is a well-controlled multi-factorial process, with multiple rate-limiting factors.

Since septins have been implicated in ER polarization in yeast [32], we sought to determine whether Sept2 depletion would affect the morphology of the ER or of other organelles, such as the Golgi apparatus and peroxisomes. The ER and Golgi morphology was not visibly altered in Sept2-depleted cells (Fig 1E). Similar mean areas were detected for the Golgi and the ER–mitochondria overlap in

Figure 1. Sept2 depletion affects mitochondrial morphology.

A Mitochondrial morphology in HeLa cells depleted of Sept2, Sept7, and Sept9. Mitochondria were labeled with Mitotracker (green). Scale bar: 10 μm. The inset represents a fourfold enlargement.

B Quantification of mean mitochondrial length in mock-treated cells and in cells depleted of Sept2, Sept7, and Sept9. Mean ± SEM, *n* > 250 individual mitochondria from three independent experiments. **$P < 0.01$, ***$P < 0.005$, ns: $P > 0.05$.

C Mitochondrial morphology in mock-treated cells or HeLa cells depleted of Sept2 and then transfected with empty vector, siRNA-resistant HA-tagged Sept2 (Sept2-rescue) or Sept7 (Sept7-rescue). Mitochondria were labeled with Mitotracker (shown in green), asterisks mark transfected cells. Scale bar: 10 μm, insets are fourfold enlargements.

D Quantification of mean mitochondrial length in mock-treated cells, in cells depleted of Sept2 or in cells depleted of Sept2 and transfected with siRNA-resistant Sept2 (Sept2-rescue) or Sept7 (Sept7-rescue). Mean ± SEM, *n* > 200 individual mitochondria from two independent experiments. ***$P < 0.005$.

E Mock-treated or Sept2-depleted U2OS cells stained for Sept2 (green) and the Golgi apparatus (GM130, red), the ER (Sec61b-GFP, displayed in red) or peroxisomes (PMP70, red). Scale bar: 10 μm, insets are enlarged twofold.

F Quantification of the mean Golgi area (mean ± SEM, *n* = 40 cells, three independent experiments).

G Quantification showing the percentage of ER traversing well-resolved mitochondrial tubules (mean ± SEM, *n* = 15 cells from three independent experiments).

H Quantification of average peroxisome counts per cell (mean ± SEM, *n* = 40 cells from three independent experiments).

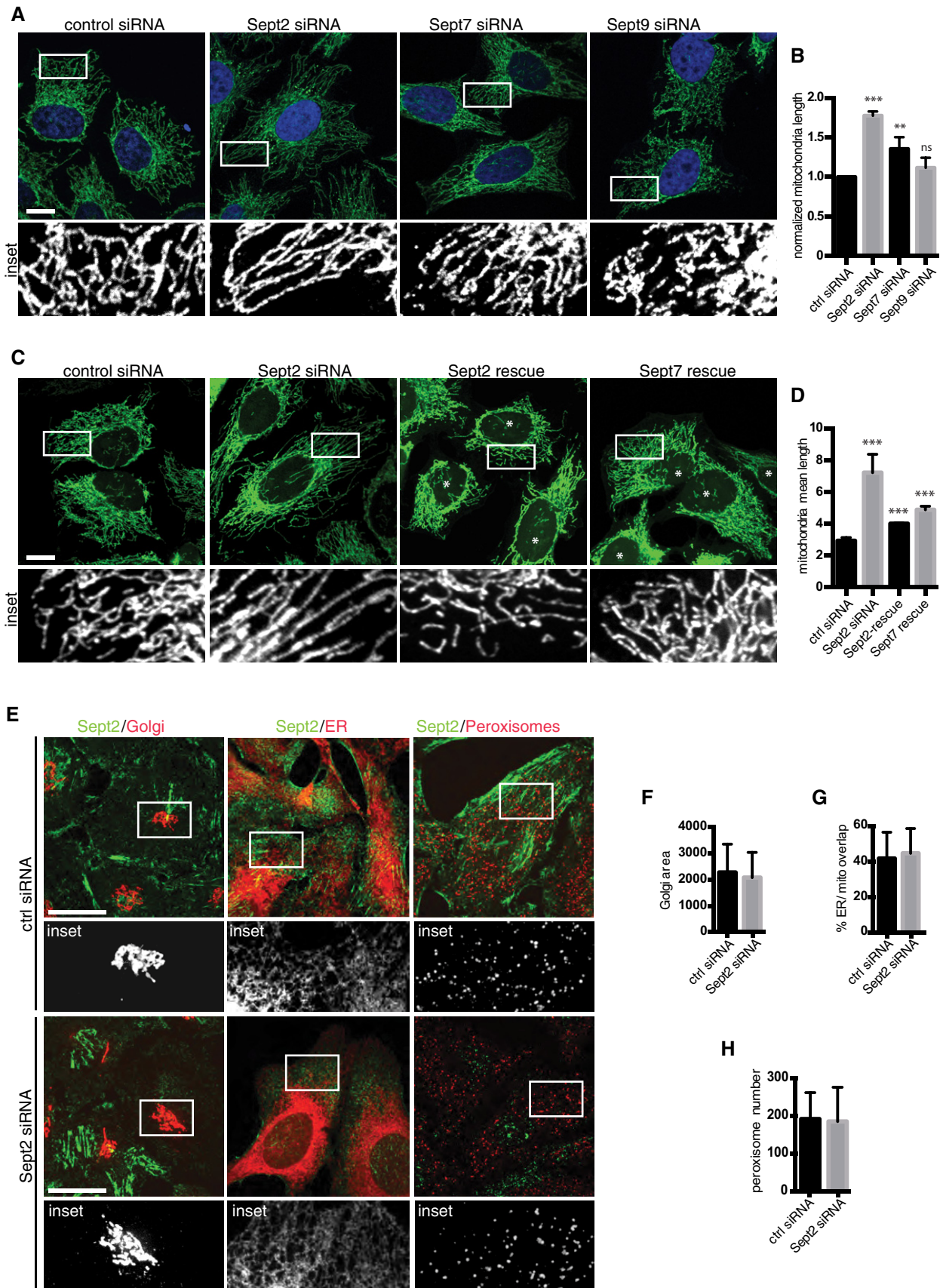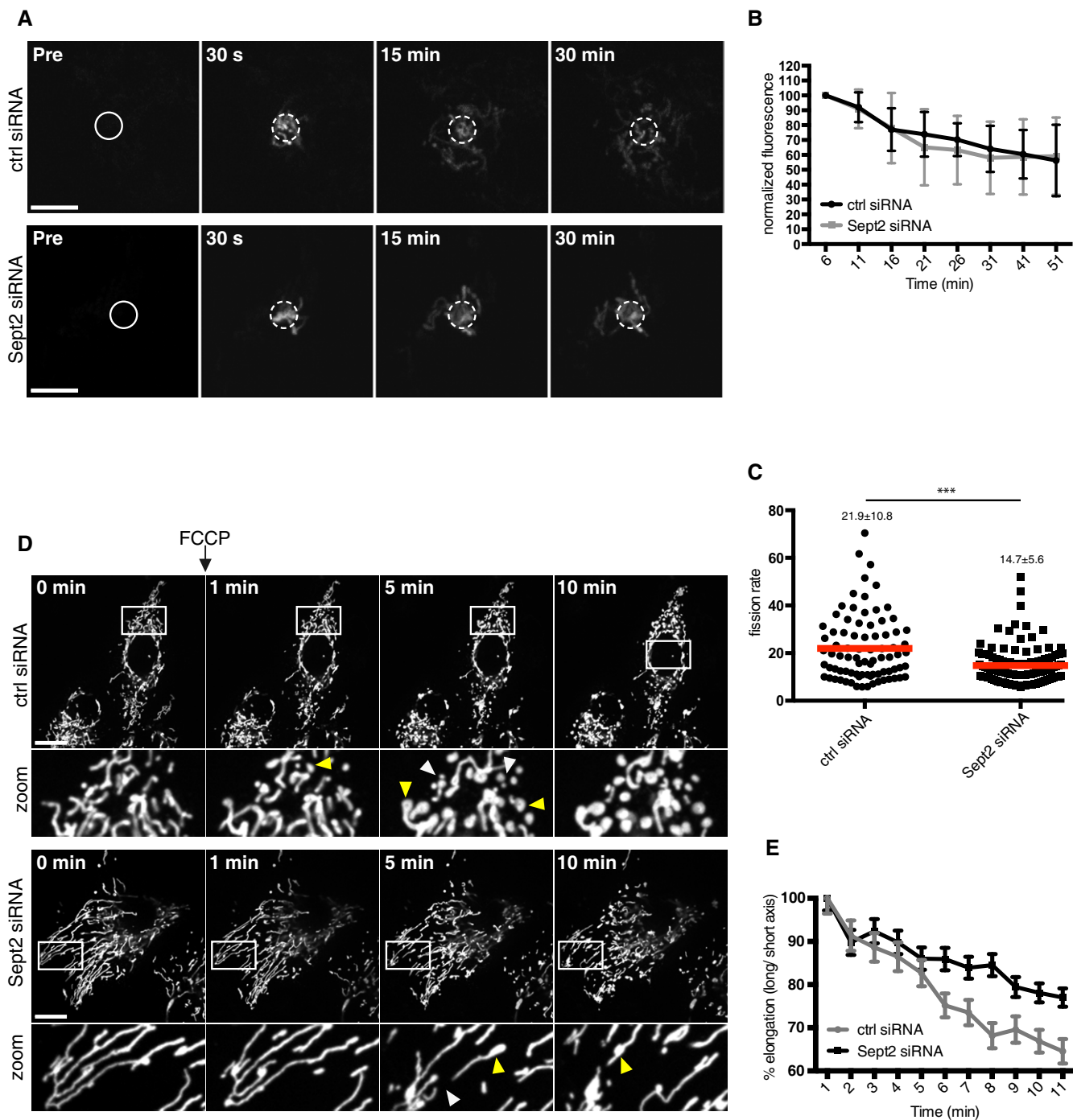Source data are available online for this figure.

Figure 1.

Figure 2. Mitochondrial dynamics in Sept2-depleted cells.

A   Live cell imaging of mock-treated or Sept2-depleted U2OS cells analyzed with the mito-PA-GFP mitochondrial fusion assay. Mito-PA-GFP is photoactivated in the indicated ROI and the decrease in fluorescence is followed in the same ROI, correcting for cell movement Scale bar: 10 μm.

B   Quantification of mitochondrial fusion rates in mock-treated or Sept2-depleted cells expressed as a means of three independent experiments ± SEM.

C   Quantification of fission rates in mock-treated and Sept2-depleted cells. Red lines indicate the mean of *n* = 116 fission events for Sept2 siRNA, *n* = 83 fission events for mock, from two independent experiments. ***P < 0.005.

D   Live cell imaging of U2OS cells stably transfected with a GFP targeted to the mitochondrial outer membrane (OM-GFP), showing delayed FCCP-induced mitochondrial fission in Sept2-depleted cells compared to mock-treated cells. White arrowheads point at fission examples, yellow arrowheads to looping. Scale bar: 20 μm, insets are enlarged fourfold.

E   Quantification of mitochondrial elongation (long/short axis) in mock-treated and FCCP-treated U2OS cells showing increased elongation in Sept2-depleted cells compared to mock-treated cells, mean of four independent experiments ± SEM.

Source data are available online for this figure.

mock- and siRNA-treated cells (Fig 1F and G). Moreover, live cell imaging showed that the ER marked mitochondrial fission sites to the same extent in control and in Sept2 siRNA-treated cells (Fig EV1G). Likewise, the number and size of peroxisomes were not significantly changed in Sept2-depleted cells compared to mock-treated cells (Fig 1E and H), suggesting that although mitochondria and peroxisomes share components of the fission machinery [13,41], Sept2 acts specifically in mitochondrial dynamics.

Sept2 does not affect fusion but controls mitochondrial fission

The mitochondrial hyperfusion phenotype could result from an increase in fusion activity or a decrease in fission. We thus tested whether Sept2 depletion would affect global levels of the key mito-chondrial dynamics proteins Mfn1/2 and Drp1. Total levels of Mfn1/2 and Drp1 were not affected by Sept2 siRNA (Fig EV2A and B). Live cell imaging revealed that Sept2-depleted cells displayed an increase in mitochondrial motility (Fig EV2C and D), which may allow more frequent encounters between mitochondria and thus higher fusion rates [15]. We therefore tested whether Sept2 stimulates mitochon-drial fusion activity. To measure the mitochondrial fusion rate, we employed an established assay, in which mitochondrial photoactivat-able GFP (mito-PA-GFP) is activated in a small region of interest, and its decay in fluorescence is followed over time to estimate the number of mitochondrial fusion events (i.e., the fusion rate), from which the fluorescence decay depends [42]. Using this assay, we could not detect any significant increase in mitochondrial fusion when compar-ing Sept2-silenced cells with mock-treated cells (Fig 2A and B).

Given that Sept2 depletion resulted in elongated mitochondria without increasing mitochondrial fusion, we analyzed whether Sept2 functionally contributes to mitochondrial fission by measuring fission rates in mock-treated and Sept2-depleted cells. Sept2-depleted cells display decreased fission rates (mean 14.8 ± 5.7) compared to mock-treated cells (21.97 ± 10.8; Fig 2C). Sept2-depleted cells also differed with respect to FCCP-induced mitochondrial fission and looping [43], which appeared delayed in Sept2-depleted cells compared to cells treated with control siRNA (Fig 2D and E). Given that FCCP-induced mitochondrial fission is Drp1-dependent [44–49], this suggests that Sept2 may play a role in Drp1-dependent mitochondrial fission.

Sept2 localizes at mitochondrial fission sites

We reasoned that given the effect of Sept2 depletion on mitochon-drial morphology and its implication in FCCP-induced mitochondrial fission, a fraction of Sept2 would localize at mitochondria to regu-late mitochondrial dynamics. We thus inspected the localization of endogenous Sept2 by confocal microscopy and found Sept2 struc-tures at mitochondria in HeLa (Fig 3A and B) and U2OS cells (Fig 3C). In addition, we detected Sept2 in a crude mitochondrial fraction (Fig EV3A). 3D image reconstruction showed that endoge-nous Sept2 localizes above and around constricted mitochondria (Fig 3B, white arrowheads). Notably, we also found constrictions that were not marked by Sept2 (Fig 3B, yellow arrowhead). This might be due to: (i) a transient association of Sept2 to mitochondrial fission sites; (ii) participation of Sept2 to only a subset of fission events, similar to what has been suggested for Myo2 and INF2 [15,18]; or (iii) that other mechanisms ensure mitochondrial constriction in parallel. To achieve a clearer view of Sept2 structures

at mitochondria we turned to super-resolution imaging, using two complementary super-resolution approaches: Bioaxial's conical diffraction (CoDiM) based super-resolution method (Fig 3C) [50] and structured illumination microscopy (SIM) (Fig EV3B). Where mitochondria were not obscured by strong cytosolic Sept2 staining, we detected Sept2 on 36% of constriction sites ($n = 209$ constriction sites), with short Sept2 structures often traversing the mitochondria in a perpendicular way (Fig 3C).

We then monitored the dynamics of Sept2-YFP localization on mitochondria and in agreement with immunofluorescence analysis found Sept2 associated with mitochondria at prospective fission sites. We detected both discrete Sept2 puncta as well as Sept2-enriched halos on prospective mitochondrial fission sites (Fig 3D). Collectively, these results indicate that Sept2 localizes to mitochon-dria and is involved in mitochondrial fission.

Sept2 interacts directly with Drp1

We then sought to determine how Sept2 would act on mitochondrial fission. Given that Drp1-dependent mitochondrial fission is delayed in Sept2-depleted cells (Fig 2D and E), we hypothesized that Sept2 might interact with Drp1. Consistent with this hypothesis, immuno-precipitation of endogenous Sept2 resulted in co-precipitation of endogenous Drp1 from cell lysates of several different human cell types (HeLa, HEK293, and U2OS), indicating *in vivo* association of Drp1 and Sept2 (Figs 4A and EV3C and D). In contrast, actin or the mitochondrial outer membrane protein Tom20 did not co-precipitate in HeLa cells (Fig 4A), nor did INF2 in U2OS cells (Fig EV3D). To further verify the specificity of the Sept2–Drp1 interaction, we immunoprecipitated an unrelated cytosolic protein (PI4KIIα) and did not recover any Drp1 (Fig EV3E). The interaction between Sept2 and Drp1 is likely to be direct because recombinant Sept2 interacted with Drp1 in GST pulldown experiments (Fig 4B). Immunofluorescence and live cell imaging confirmed that Sept2 and Drp1 can be found together at mitochondria (Fig 4C) and at mitochondrial fission sites (Fig 4D). We noticed that the two proteins do not colocalize at all prospective fission sites, suggesting that either the Sept2–Drp1 complex forms very transiently, or that Sept2 is below the detection level at these sites, or that Drp1 is recruited to mitochondria through several independent pathways. To investigate whether the Drp1–Sept2 interaction occurred preferentially in the cytoplasm or on mito-chondria, we treated cells with CCCP to increase Drp1 localization to mitochondria. Treatment with CCCP caused a twofold increase in Drp1 binding to Sept2, suggesting that formation of the Sept2–Drp1 complex is stimulated at mitochondria (Fig 4E and F). We next asked whether the interaction between Sept2 and Drp1 was sensitive to the activation state of Drp1. We thus treated cells with Mdivi-1, which inhibits self-assembly and GTPase activity of Drp1, resulting in increased interconnectivity of the mitochondrial network [51] (Fig EV4F) without depolymerizing Sept2 filaments (our unpublished results), and then performed Sept2 immunoprecipitation. Mdivi-1 treatment decreased the association between Sept2 and Drp1 by almost 50% in intact cells (Fig 4G and H), and partially decreased the Sept2–Drp1 interaction in an *in vitro* pulldown assay (Fig EV3G).

Together, these data establish that Sept2 directly interacts with Drp1 *in vivo* and *in vitro* and suggest that the activation state of Drp1, its assembly, or the molecular environment on the mitochon-drial outer membrane may stabilize the Sept2–Drp1 complex.
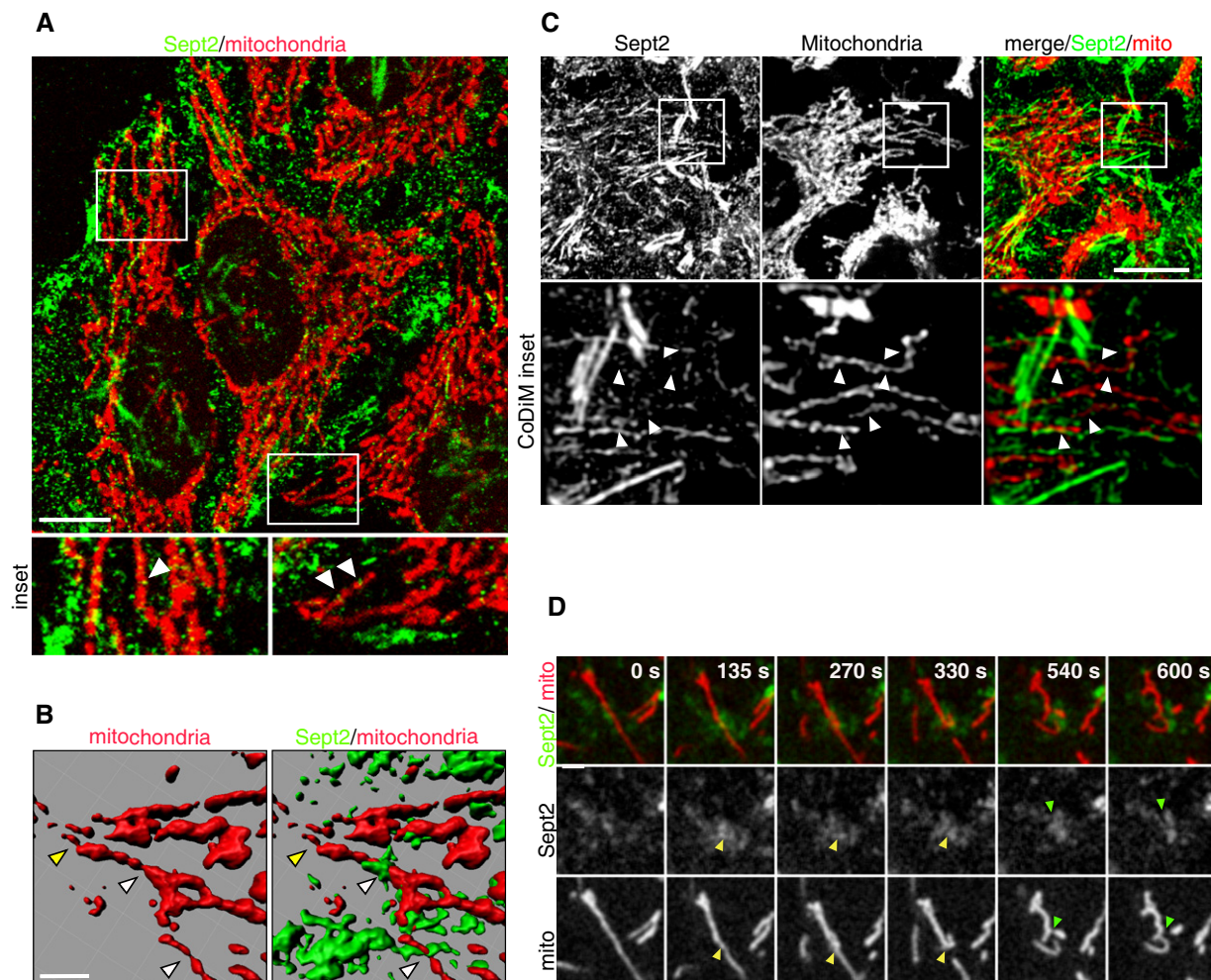
Figure 3. Sept2 localizes to mitochondrial constrictions.

A   Immunofluorescence analysis of endogenous Sept2 (green) and mitochondria (Tom20, red) in HeLa cells. The insets show a twofold enlargement with arrowheads highlighting the presence of small Sept2 structures on mitochondria. Scale bar: 10 μm.

B   3D rendering of confocal sections showing Sept2 at mitochondrial constrictions (white arrowheads) and constricted mitochondria that are not marked by Sept2 (yellow arrowheads). Scale bar: 2 μm.

C   CoDiM super-resolution imaging of endogenous Sept2. Arrowheads highlight the presence of Sept2 at mitochondrial constrictions. Insets show a threefold enlargement Scale bar: 10 μm.

D   Still images from a live cell imaging experiment showing Sept2 (green) accumulation during two mitochondrial fission events (Mitotracker orange, red), highlighted by yellow (first fission) or green arrowheads (second fission). Scale bar: 2 μm.

Source data are available online for this figure.

Mitochondrial localization of Drp1 depends on Sept2

Since Sept2 interacts with Drp1, we analyzed the effect of Sept2 depletion on the mitochondrial localization of Drp1 complexes. Immunofluorescence analysis showed that the amount of mitochondria-associated Drp1 significantly decreased in Sept2-silenced cells (67% ± 15.1) compared to mock-treated cells (Fig 5A and B). In concomitance, the average distance between Drp1 clusters increased by a factor of 1.6 in Sept2-silenced cells (Fig 5C), indicating a decrease in Drp1 cluster density along mitochondria. In addition, Western blotting analysis of mitochondria isolated from cells treated with control siRNA or with Sept2 siRNA confirmed a decrease in the amount of mitochondria-associated Drp1 (Fig 5D). These data

suggest that Sept2 acts upstream of Drp1, similar to what has been recently shown for INF2 and Myo2 [15,18]. In agreement with this finding, Drp1 depletion did not affect Sept2 levels or subcellular distribution, as assessed by immunofluorescence (our unpublished results). Altogether, our observations revealed that Sept2 participates to the localization of Drp1 complexes on mitochondria.

Mitochondria-associated actomyosin is not perturbed upon Sept2 depletion

Actin and myosin 2 (Myo2) have been recently proposed to act together in mitochondrial preconstriction, favoring Drp1 accumulation in order to accomplish fission [18]. Myo2 had also been shown
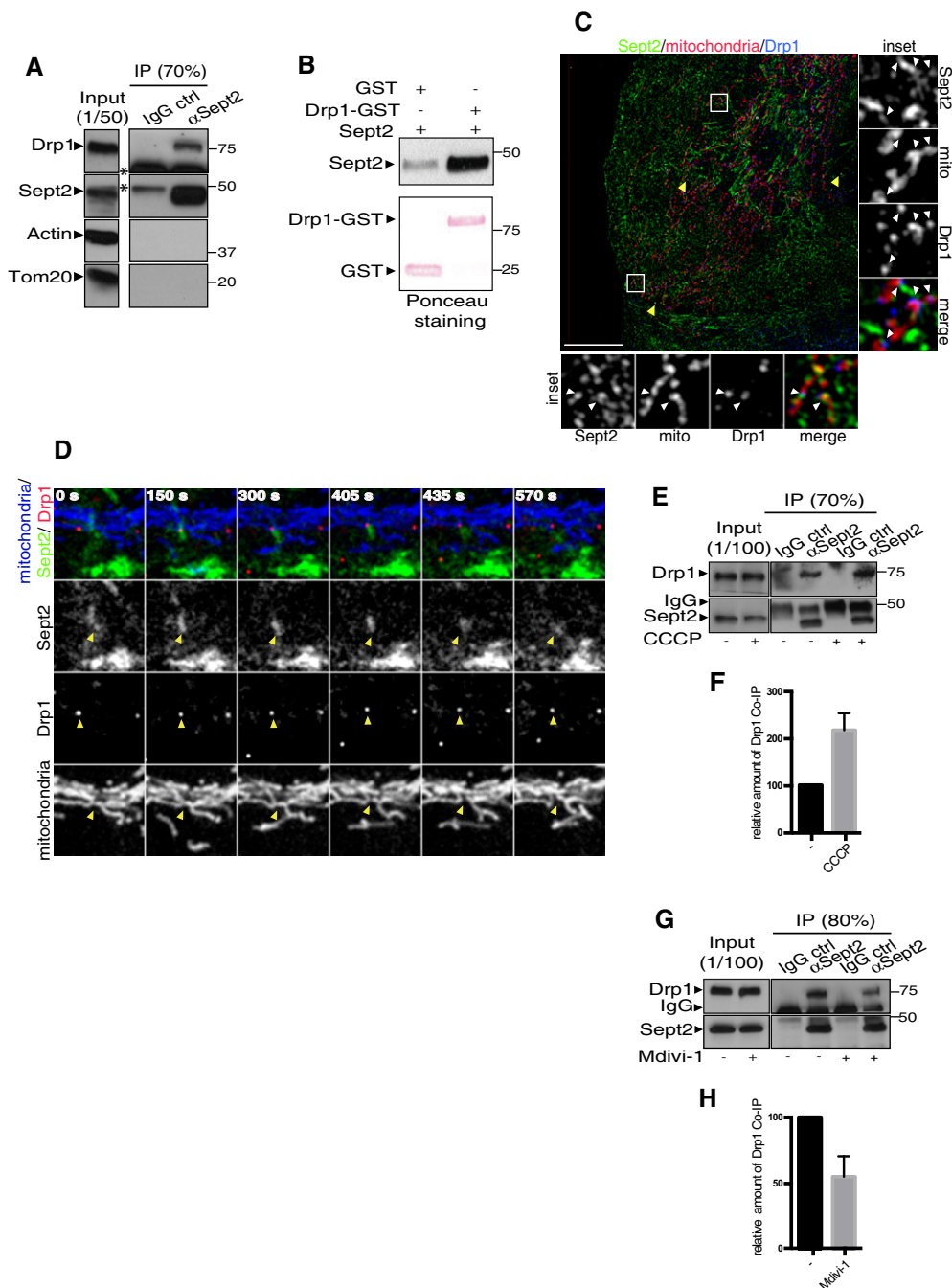
Figure 4. Sept2 interacts with Drp1.

A   Western blot analysis of endogenous Sept2 immunoprecipitation from HeLa cells showing that endogenous Drp1 specifically co-immunoprecipitates with Sept2. The asterisks mark the IgG heavy chains.

B   GST pulldown of recombinant Sept2 with GST-Drp1 or GST alone showing that Sept2 is able to interact directly with Drp1.

C   Elyra SIM image of U2OS cells stained for Sept2 (green), mitochondria (GFP targeted to the outer membrane (OM-GFP), shown in red), Drp1 (blue). Yellow arrows point at TetraSpeck beads used for image alignment. Insets represent sevenfold enlargements. White arrows in the insets point to sites where Drp1 and Sept2 colocalize on mitochondria. Scale bar: 10 μm, insets are enlarged fourfold.

D   Snapshots of a live cell imaging experiment in U2OS cells showing Sept2 (green, Sept2-YFP), Drp1 (red, Drp1-mCherry) and mitochondria (blue, Mitotracker DeepRed) during mitochondrial fission. Merged and single channels show the dynamics of Sept2 and Drp1 during mitochondrial fission (yellow arrowheads). Scale bar: 2 μm.

E   Sept2 immunoprecipitation from mock or CCCP-treated HeLa cells probed for Drp1 and Sept2.

F   Quantification of two independent experiments showing stimulated Drp1 co-immunoprecipitation with Sept2 in FCCP-treated cells.

G   Sept2 immunoprecipitation from mock or Mdivi-1-treated HeLa cells probed for Drp1 and Sept2.

H   Quantification of two independent experiments showing decreased Drp1 co-immunoprecipitation with Sept2 upon Mdivi-1 treatment.

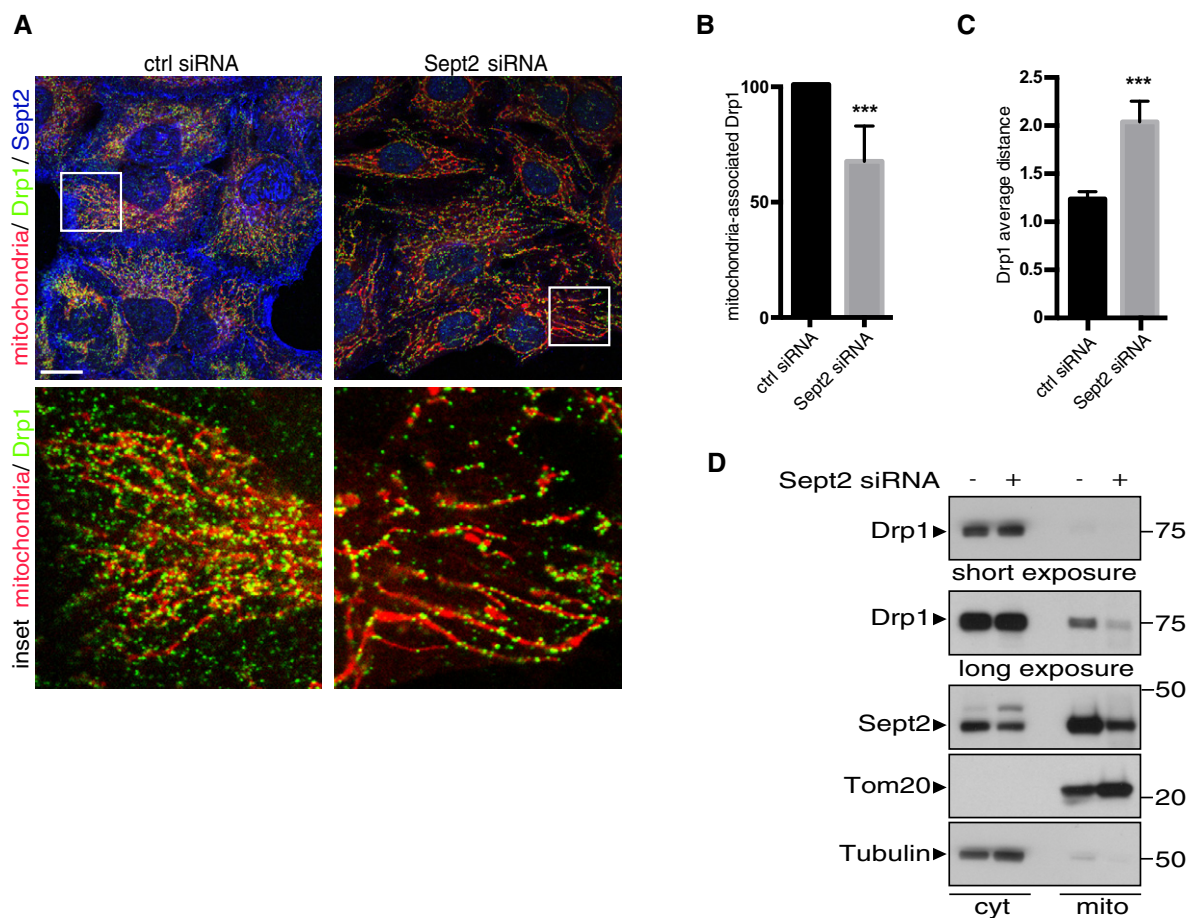Source data are available online for this figure.

Figure 5. Sept2 is required for efficient recruitment of Drp1 to mitochondria.

A Immunofluorescence of Sept2 (blue), mitochondria (Tom20, red), and Drp1 (green) in mock-treated and Sept2-depleted cells. Scale bar: 10 μm, insets are enlarged fourfold.
B Quantification of mitochondria-associated Drp1 in mock-treated and Sept2-depleted cells (mean of 3 independent experiments ± SEM, n = 44–51 cells).
C Average distance between mitochondria-associated Drp1 oligomers (mean ± SEM, representative experiment with n > 25 individual mitochondria, ***P < 0.005).
D HeLa cytosol and crude mitochondrial fractions prepared from mock- and Sept2 siRNA-treated cells. The samples were analyzed by Western blotting with the indicated antibodies, and show a decrease in mitochondria-associated Drp1 in Sept2-depleted cells.

Source data are available online for this figure.

previously to directly bind Sept2 [19]. This binding was required for phosphorylation-dependent activation of Myo2, which played an important role in stress fiber maintenance and during cytokinesis [19]. However, whether the Sept2–Myo2 interaction can also occur at mitochondria and/or have a functional role in mitochondrial dynamics is unknown to date. Therefore, we explored whether Sept2 depletion would alter Myo2 localization at mitochondria or decrease its activation. We neither detected changes in total Myo2A or Myo2B levels (Fig EV4A and B) nor a decrease in the levels of phosphorylated regulatory myosin light chain (P-MLC and PP-MLC; Fig EV4C–F), which determines the actin-binding properties of Myo2 in Sept2-silenced cells [52]. We also failed to detect a significant change in mitochondria-associated P-MLC by immunolocalization (Fig 6A and B). We thus concluded that the mitochondrial elongation observed in Sept2-depleted cells is not due to perturbation of Myo2 levels or activity.

Notably, P-MLC has been shown to localize to mitochondria in an actin-dependent manner [18]. The lack of P-MLC redistribution

in Sept2-depleted cells suggests that the interaction of actin with mitochondria is not perturbed in this context. In agreement with this observation, we found that Sept2 depletion did not interfere with the induction of actin recruitment to mitochondria upon FCCP treatment [17] (Fig 6C). In addition, we examined whether Sept2 depletion would affect the mitochondrial localization of the actin-binding proteins Arp3, cofilin, and cortactin, which were recently shown to regulate mitochondrial morphology [17]. Immunofluorescence and cell fractionation experiments showed that the mitochondrial association between Arp3, cofilin, and cortactin was not affected in Sept2-depleted cells (Fig 6D and E).

We next tested whether the interaction between Sept2 and Drp1 requires actin polymerization by treating cells with cytochalasin D prior to immunoprecipitation and found that the Sept2–Drp1 interaction was not affected (Fig 6F). Together, these results indicate that Sept2 is not involved in the recruitment of actin and Myo2 at mitochondria and that the interaction between Sept2 and Drp1 is independent of actin dynamics.

Septin contribution to mitochondrial dynamics is conserved in *C. elegans*

To understand whether the septin contribution to mitochondrial dynamics is conserved among metazoa, we turned to *C. elegans*, which possesses only two septins, *UNC-59* and *UNC-61*. We inspected mitochondrial morphology in body wall muscle cells, a well-established model to assess mitochondrial dynamics phenotypes [53–55]. Knockdown of either *UNC-59* or *UNC-61* or both by siRNA dramatically affected mitochondrial morphology, causing an increase in mitochondrial branching and length (Figs 7A and B, and EV5A and B) that is reminiscent of fission protein knockdown [54–56]. We then assessed whether combining the depletion of septins with the depletion of Drp1 would result in a further increase in mitochondrial length, which would indicate that the two proteins act on mitochondria through different pathways. We chose to focus on *UNC-61,* whose depletion results in a stronger mitochondrial phenotype compared to *UNC-59,* and co-silenced it with *DRP-1.* The strong mitochondrial phenotype of *DRP-1*(RNAi) worms was not exacerbated when *UNC-61* was co-silenced, suggesting that the phenotypes induced by *DRP-1* and *UNC-61* knockdown are not additive (Fig 7C). These data are consistent with the phenotype observed in mammalian cells and suggest that the function of septins in mitochondrial dynamics is conserved in *C. elegans*.

Discussion

Mitochondrial fission is a highly regulated process, and recent progress has highlighted novel roles for several cellular components in this process, such as the ER, actin, and multiple actin-binding proteins [15–18,43,57]. Here, we add a new player to this complex picture and report on the role of septins, a component of the cytoskeleton, in mitochondrial dynamics. We describe that septin expression is important for mitochondrial morphology in human cell lines and in the nematode *C. elegans*. In human cells, depletion of three ubiquitously expressed septins (Sept2, Sept7, and Sept9) showed that both Sept2 and Sept7 are important for mitochondrial fission, as their depletion induces significant mitochondrial elongation. In line with previous results [33,38,39], we found that that depletion of Sept7 partially codepletes Sept2. The remaining Sept2 may account for the decreased penetrance of the mitochondrial phenotype in Sept7-silenced cells compared to Sept2-silenced cells.

Furthermore, the small levels of Sept2 remaining after Sept2 siRNA may serve as seeds that allow Sept7 to partially rescue the mitochondrial phenotype when overexpressed in Sept2-silenced cells. In contrast, Sept9 depletion did not induce mitochondrial elongation, but appeared to increase mitochondrial interconnectivity, similar to nocodazole treatment [43,58]. We speculate that the differences between Sept2/7 and Sept9 may be related to the position of Sept9 in the septin heterocomplex [59] or to the presence of Sept2-containing complexes in Sept9-depleted cells that still act on mitochondria. Such Sept2-containing complexes were previously shown to form short filaments in Sept9-depleted cells [59]. In agreement with this, we did not detect Sept2 codepletion in Sept9-silenced cells.

In our hands, Sept2 presented the most dramatic mitochondrial phenotype, raising the question of how Sept2 mechanistically impacts mitochondrial dynamics. We propose that Sept2 plays a role in Drp1-dependent mitochondrial fission. This notion is supported by several observations: First, mitochondrial association of Drp1 is impaired in Sept2-depleted cells. Second, FCCP-induced mitochondrial fission, which is Drp1-dependent, is delayed in Sept2-depleted cells. Lastly, Sept2 interacts directly with Drp1. An indirect confirmation of our results is the recent finding that Sept5 and Sept11 bind dynamin in neuronal cells [60]. The high homology of dynamin and Drp1 suggests that their interaction with septins may be ancestral. The interaction between Sept2 and Drp1 appears to require Drp1 assembly or activation, as it is sensitive to Mdivi-1, which has been shown to inhibit the Drp1 assembly-dependent GTPase activity [51]. In our hands, the effect of Mdivi-1 was stronger *in vivo* than *in vitro,* indicating that the molecular environment on the mitochondrial outer membrane may stabilize the Sept2–Drp1 complex.

In contrast, Sept2-mediated GTP hydrolysis may be dispensable for this interaction, as overexpression of a GTPase-deficient point mutant (Sept2-T78G) did not affect mitochondrial morphology (our unpublished results), consistent with the very low rate of GTP hydrolysis that has been observed by others in septin heterooligomers [61,62] and which appears to be due to the low solvent accessibility of the nucleotide-binding pocket [63].

We propose alternative but not mutually exclusive scenarios that could account for the role of Sept2 in Drp1-dependent mitochondrial fission. Sept2 could promote Drp1 recruitment by contributing to mitochondrial constriction. Alternatively, Sept2 might stabilize productive fission complexes or act as a scaffold that promotes Drp1 recruitment or retention on mitochondria, as has been proposed for

Figure 6. Sept2 does not affect mitochondrial Myo2 localization and does not require actin dynamics for interacting with Drp1.

A   Immunofluorescence analysis of P-MLC (green) recruitment to mitochondria (red, Tom20) in mock-treated and Sept2-depleted HeLa cells. Insets show twofold enlargements. Scale bar: 10 μm.

B   Colocalization of P-MLC with mitochondria was assessed with Icy software and showed no difference between mock-treated and Sept2-depleted cells (mean ± SEM).

C   Mock-treated or Sept2-depleted Drp1$^{-/-}$ MEF cells were labeled with Mitotracker orange (red), treated for the indicated amount of time with 2 μM FCCP and stained for actin with phalloidin (green). Insets are enlarged twofold. Scale bar: 10 μm.

D   Immunofluorescence analysis of the actin-binding proteins Arp3 and cofilin (green) colocalized with cytochrome c (red), and cortactin (green) colocalized with Hsp60 (red) in mock-treated or Sept2-depleted Drp1$^{-/-}$ MEF cells. Scale bars: 10 μm.

E   Cytosol and crude mitochondria fractions were prepared from mock-treated or Sept2-depleted Drp1$^{-/-}$ MEF cells and analyzed by Western blotting with the indicated antibodies.

F   HeLa cells were mock-treated or treated with cytochalasin D and subjected to Sept2 immunoprecipitation. Immunoprecipitates were analyzed by Western blot for Drp1 and Sept2, showing that Drp1 co-immunoprecipitation with Sept2 is not affected by cytochalasin D treatment.

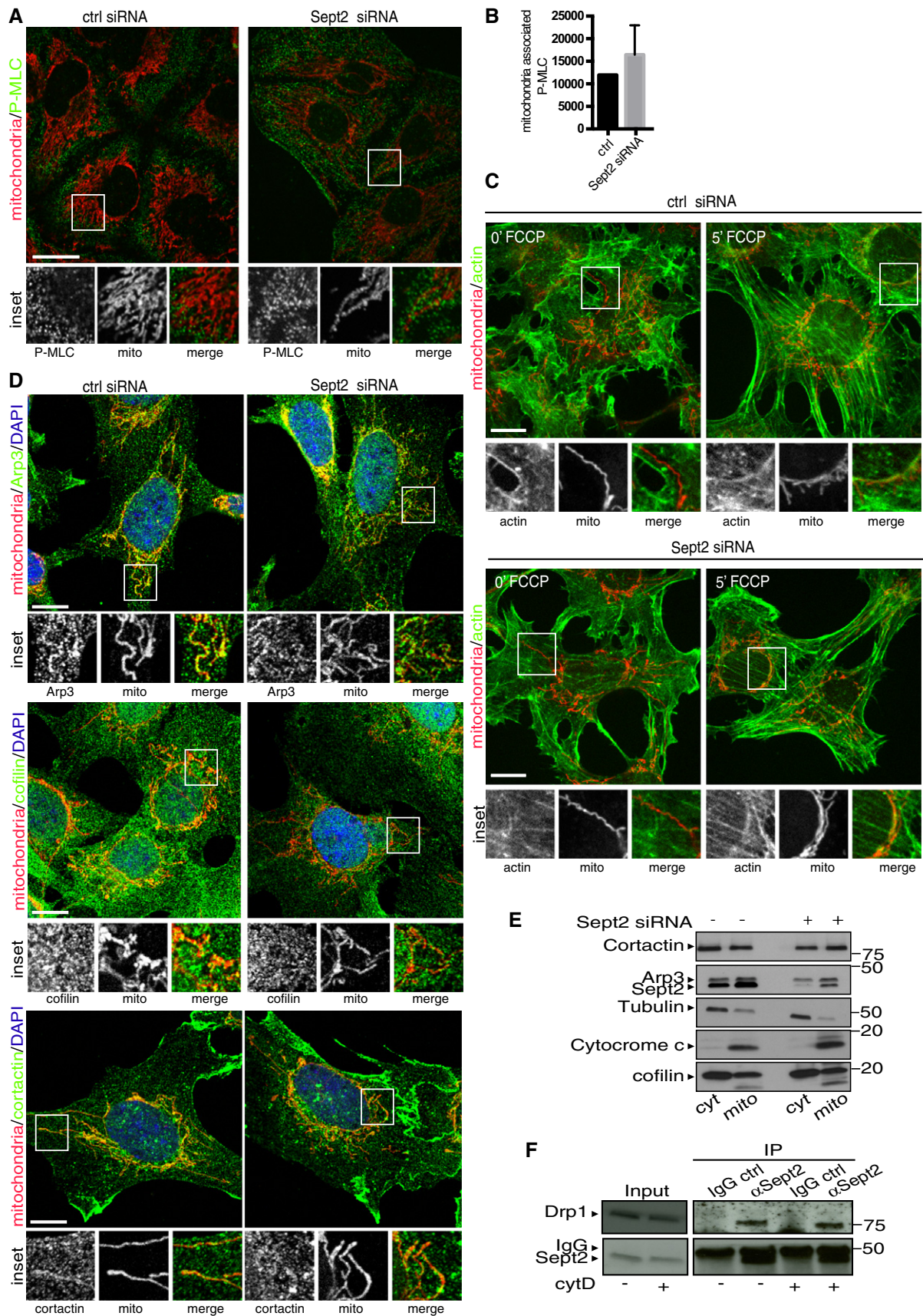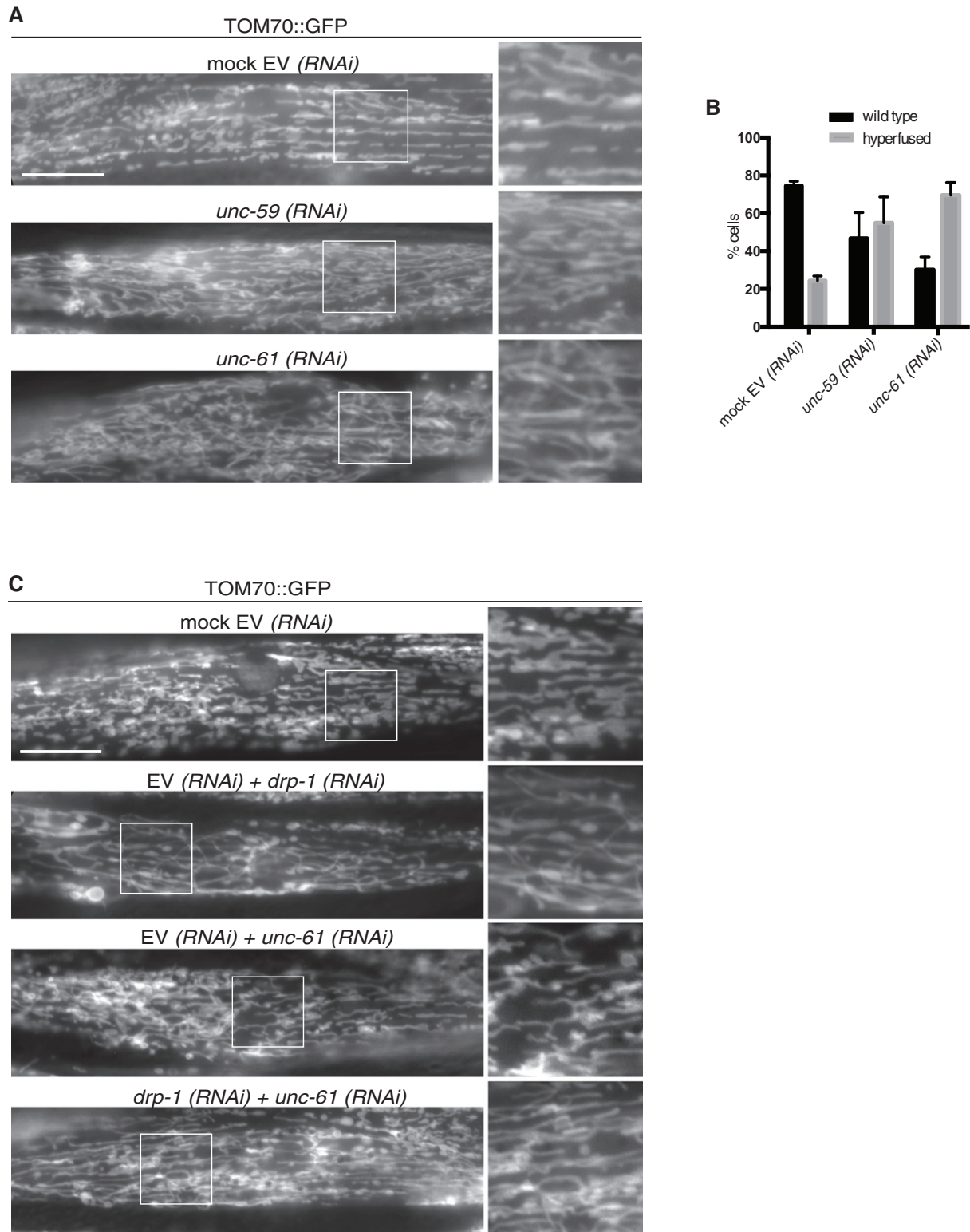Source data are available online for this figure.

Figure 6.

A TOM70::GFP

mock EV *(RNAi)*

unc-59 (RNAi)

unc-61 (RNAi)

B

C TOM70::GFP

mock EV *(RNAi)*

EV *(RNAi) + drp-1 (RNAi)*

EV *(RNAi) + unc-61 (RNAi)*

drp-1 (RNAi) + unc-61 (RNAi)

Figure 7. Mitochondrial structure in muscle cells is affected upon knockdown of *UNC-59* and *UNC-61*.

A, B   Live imaging of *C. elegans* expressing TOM70::GFP in body wall muscle cells. Depletion of the *UNC-59* or *UNC-61* led to an increase in mitochondrial network connectivity as shown by the quantification of four independent experiments in (B) (mean ± SEM). Insets represent a twofold magnification. Scale bar: 10 μm.

C   Live imaging of *C. elegans* body wall muscle cells expressing TOM70::GFP. Depletion of *DRP-1* or *UNC-61* caused an increase in mitochondrial elongation and network connectivity, which did not increase upon combination of *DRP-1* and *UNC-61*. Insets represent a twofold magnification. Scale bar: 10 μm.

Source data are available online for this figure.

actin [43,57]. Notably, despite the fact that septins can use actin as an assembly template and partially colocalize with actin [33], we suspect that Sept2 does not play a substantial role in actomyosin driven mitochondrial fission [18]. In agreement with this hypothesis, actin and INF2 were not detected in Sept2 immunoprecipitations and cytochalasin D treatment had no effect on the Sept2–Drp1 interaction, the latter suggesting that it does not require actin polymerization. Furthermore, neither the total levels of Myo2A, Myo2B, P-MLC or PP-MLC, nor the localization of P-MLC on mitochondria, which relies on actin, are affected in Sept2-depleted cells. P-MLC and PP-MLC were reported to decrease in previous Sept2-depletion experiments [19], a variation that may be explained by differences in the employed cell types (CHO-K1 versus HeLa and U2OS) or silencing techniques (shRNA versus siRNA). Interestingly, Li *et al* [17] reported increased Drp1 recruitment to mitochondria upon depletion of the actin regulating proteins Arp3, cortactin, and cofilin, while we observe a decreased localization of Drp1 to mitochondria in Sept2-depleted cells and no substantial difference in mitochondrial localization of Arp3, cortactin, and cofilin. Consistent with our findings, FCCP-induced recruitment of actin to mitochondria was also preserved in Sept2-depleted cells.

Our data support the view that multiple mechanisms regulate mitochondrial fission. On the one hand, accumulating evidence suggests the presence of Drp1-independent fission mechanisms [48,64]. On the other hand Drp1 is regulated in a highly complex manner, that is, through several Drp1 receptors on mitochondria, through posttranslational regulation of Drp1 itself, and through the regulated recruitment of Drp1 to mitochondria by its receptors Fis1, Mid49/51, and Mff [11,12] [10,13,14,65,66]. The recruitment and activity of Drp1 on mitochondria is furthermore regulated by cellular structures such the ER [67] and actin [15,18,43,57], as well as septins, which appear to function in parallel to the ER and actin. Hence, the mitochondrial fission process appears to be regulated in complex and at least partially redundant ways. Such redundancy is frequently observed in biological systems and is thought to contribute to their robustness. Although not the only means to recruit Drp1 to mitochondria, Sept2 has in contrast to the ER and actin the unique ability to directly bind Drp1. This could allow Sept2 to act as a scaffold that would promote functional interactions with other proteins on mitochondria, similar to the function that septins have already been shown to fulfill in other contexts such as cytokinesis [19]. Our findings thus unveil a new facet of Drp1 regulation and expand the role of the cytoskeleton in mitochondrial fission to septin proteins.

Materials and Methods

Cell culture and transfection

HeLa and U2OS cells were obtained from ATCC and cultured under standard conditions; media and additives were from Invitrogen. U2OS-GFPSec61 stable cells were described previously [68], as well as Drp1$^{-/-}$ cells [45]. All cells were tested for mycoplasma (negative). siRNAs were transfected for 72 h at a final concentration of 12 nM with Lipofectamine RNAiMAX according to the manufacturer's instructions. Septin siRNA sequences and providers are detailed in Appendix Table S1; siRNA#1 and siRNA#2 were employed

for Figs 1 and EV1A and B, while siRNA#1 is shown in subsequent experiments. For rescue experiments, HeLa cells were transfected with Sept2 siRNA (siRNA #1) for 48 h and then transfected for a further 24 h (using FuGENE) with a Sept2-HA plasmid carrying silent mutations in the siRNA seed region (Sept2-HA rescue; see Appendix Table S2) or its GTPase-deficient derivative (carrying the T78G mutation [63]) or Sept7-HA.

Reagents

Plasmids, chemicals, and recombinant proteins

Sept2-HA template for cloning of siRNA-resistant Sept2-HA was provided by David Ribet. See Appendix Table S2 for construct and primer information. PA-GFP and Sept2-YFP were described previously [42,69]. Orange and Deep Red Mitotracker, 100 nm Tetra-Speck beads AlexaFluor-labeled phalloidin and secondary antibodies were purchased from Invitrogen. Mdivi-1 was obtained from Enzo Life Sciences, and all other chemicals were obtained from Sigma. Complete mini EDTA-free protease inhibitor and PhosSTOP phosphatase inhibitor tablets were from Roche. Reduced glutathione was obtained from Sigma, and glutathione sepharose beads and protein A were from GE Healthcare. Recombinant purified GST and Drp1-GST were prepared as described previously [70], and Sept2 was obtained from Cusabio (CSB-EP617994HU).

Antibodies

Antibody sources are detailed in Appendix Table S3. All antibodies were used according to the manufacturer's instructions unless otherwise stated.

Cell fractionation, immunoprecipitations, and pulldown

Crude mitochondrial extracts were obtained through cell fractionation according to [71]. Immunoprecipitation was performed as described [29] with modifications. Briefly, HeLa cells were washed twice in phosphate-buffered saline (PBS) and lysed for 30 min with 1 ml lysis buffer/10-cm dish (20 mM Tris, pH 8.0, 150 mM NaCl, 10% glycerol) supplemented with 1% Igepal, protease, and phosphatase inhibitors. Lysis and all subsequent steps were performed at 4°C. The lysate was clarified (13,000 *g*, 10 min), and the protein concentration of the supernatant was determined by Bradford assay (Pierce). One milligram of lysate was incubated overnight with 2 µg of anti Sept2 antibody. A total of 30 µl of protein A–sepharose beads was added for 1 h, and the immune complexes were retrieved by centrifugation (500 *g*, 5 min). After four washes with lysis buffer, bound protein was eluted from the beads by boiling for 10 min in 30 µl Laemmli buffer. The eluate was analyzed by gradient SDS–PAGE (Bio-Rad) and subjected to Western blotting via wet transfer to 0.45-µm nitrocellulose membrane (Millipore). A total of 10 µg total lysate was loaded (corresponding to 1/100) for the input, 70–90% immunoprecipitated material to reveal interactors such as Drp1, or 5% immunoprecipitated material to reveal immunoprecipitated Sept2. Sept2 immunoprecipitations from drug-treated cells were performed as above except that cells were either mock-treated (DMSO or ethanol, respectively) or treated with either 50 µM Mdivi-1 for 1 h (Mdivi-1 was also included in the lysis buffer) or 2 µM CCCP for 30 min in MEM without serum, or 2 µM cytochalasin D for 30 min in MEM before cell lysis.

GST pulldown

All steps were performed at 4°C. Equimolar concentrations of GST, GST-Drp1 and Sept2 (500 nM) were incubated overnight in GST incubation buffer (20 mM Tris, pH 8.0, 1 mM EDTA, 0.2% Igepal, 100 mM KCl). A total of 30 μl of protein A–sepharose beads was added for 1 h; beads were then recovered by centrifugation (500 *g*, 5 min) and washed four times in GST incubation buffer. Bound protein was eluted from glutathione Sepharose beads with GST elution buffer (100 mM Tris, pH 8.0, 20 mM glutathione, 5 mM dithiothreitol). Eluates were analyzed as described above. To test the effect of Mdivi-1 on the Drp1–Sept2 interaction, Drp1-GST was preincubated with Mdivi-1 for 30 min at RT before the addition of recombinant Sept2, followed by the pulldown procedure described above.

Imaging and image analysis

Immunofluorescence and live cell imaging were performed essentially as described in [48,72]. For super-resolution microscopy, cells were seeded onto high-precision coverslips (Marienfeld), and after immunofluorescence, samples were mounted in Slow-Fade Gold (Invitrogen) or Fluoromount G. Super-resolution structured illumination (SR-SIM), providing an expected resolution of about 140 nm, was performed on a Zeiss LSM780 Elyra PS1 (Carl Zeiss, Germany) using 63×/1.4 oil Plan Apo objective. Three angles of the excitation grid with five phases each were acquired for each channel and each z-plane. SIM images were processed with ZEN software for brightness/contrast adjustment. Images were aligned using 100 nm TetraSpeck beads embedded in the sample. The confocal image in Fig EV3B was acquired using the same equipment as the SR-SIM and the same pixel size to allow comparison. Huygens professional software was used for deconvolution and brightness/contrast in Fig EV3B. CoDIM imaging was performed on a Bioaxial CoDiM 100 system equipped with 488, 561, and 640 lasers and decreases the resolution limit to about 80–100 nm. Imaris 6.4.1 (Bitplane) was used for 3D reconstructions.

Image analysis was performed with ImageJ unless otherwise stated. For morphometric analysis on fixed cells, mitochondrial length was assessed in well-resolved mitochondria only; fissions were counted manually in live cell imaging experiments and displayed according to [57]. To calculate the percentage of rescue, the difference in mitochondrial length between Sept2-siRNA and Sept2-rescue or Sept7-rescue is referred to the difference between Sept2-depleted and mock-treated cells (set to 100%). To quantify FCCP-induced mitochondrial fission and looping, mitochondrial elongation (long/short axis) was measured with the open-source software Icy [73] (protocol *Mitochondria Elongation*) after binarization of mitochondria. The first timepoint (t0) was set to 100%, and the following timepoints were normalized to t0. Mitochondrial constrictions were determined through visual inspection of the mitochondrial channel, and then, septin presence was assessed at these sites. Total mitochondrial motility was determined in ImageJ according to [74]. Peroxisomes were counted automatically with ImageJ particle analyzer. The percentage of ER crossing mitochondria was assessed after thresholding and binarization of the ER and mitochondrial signal according to [67]. Similarly, mitochondrial Drp1 was obtained by combining total Drp1 signal with a mitochondrial mask created after thresholding and binarization of the mitochondrial signal. Colocalization of P-MLC was assessed similarly and verified using the plug-in *Colocalization Studio* (Plug-in ID: ICY-H9X6X2) [75] in Icy. Western blot quantification involved densitometric analysis of single bands through ImageJ. At least two Western blots from independent experiments were quantified.

Statistical analysis

Results are expressed as means of at least two independent experiments, and error bars represent the standard error of the mean. For multiple comparisons, data were first analyzed by one-way ANOVA on BiostaTGV (http://marne.u707.jussieu.fr/biostatgv/?module = tests), followed by pairwise comparisons with unpaired two-tailed Student's *t*-test on Excel (Microsoft) or Prism (GraphPad). Significance is indicated as $P < 0.05$ (*), $P < 0.01$ (**), and $P < 0.005$ (***), ns for $P > 0.05$.

C. elegans work

Caenorhabditis elegans was cultured and maintained as described previously [76] at 20°C. The worm line carrying pMyo3::Tom70:: GFP, rol-6 as extrachromosomal array was created previously [54]. RNAi was performed as described [77]. Plasmid L4440 containing *unc-59* (W09C5.2) or *unc-61* (Y50E8A.4) was retrieved from the Ahringer library [77] or the Vidal library [78], respectively. Both clones were sequenced to confirm their identity. For the double RNAi and the dilution controls, equal volumes of bacterial cultures were mixed, concentrated by centrifugation, and spread on NGM plates containing 1.5 mM IPTG and 25 μg/ml carbenicillin. dsRNA production was induced at RT for 16–24 h and then stored at 4°C for up to 2 weeks. TOM70::GFP worms were subjected to RNAi from L3/L4 stage for 4–5 days at 20°C. Offspring were analyzed at young adult stage. For live imaging, adult hermaphrodites were mounted in M9 containing 1 mM levamisole (Sigma-Aldrich), using Vaseline® at the edges of the coverslip to function as a spacer. Worms and mounting medium were strictly kept at 20°C until use. Images were taken at a Zeiss Axioplan 2 microscope equipped with a Zeiss AxioCam MRm camera (Carl Zeiss, Germany) and a Plan Neofluar 100×/NA1.30 oil objective.

Expanded View for this article is available online.

Conflict of interest

The authors declare that they have no conflict of interest.

References

1. Anesti V, Scorrano L (2006) The relationship between mitochondrial shape and function and the cytoskeleton. *Biochim Biophys Acta* 1757: 692–699

2. Mishra P, Chan DC (2014) Mitochondrial dynamics and inheritance during cell division, development and disease. *Nat Rev Mol Cell Biol* 15: 634–646

3. Labbe K, Murley A, Nunnari J (2014) Determinants and functions of mitochondrial behavior. *Annu Rev Cell Dev Biol* 30: 357–391

4. Kasahara A, Scorrano L (2014) Mitochondria: from cell death executioners to regulators of cell differentiation. *Trends Cell Biol* 24: 761–770

5. Nunnari J, Suomalainen A (2012) Mitochondria: in sickness and in health. *Cell* 148: 1145–1159

6. Elgass K, Pakay J, Ryan MT, Palmer CS (2013) Recent advances into the understanding of mitochondrial fission. *Biochim Biophys Acta* 1833: 150–161

7. Chang CR, Blackstone C (2010) Dynamic regulation of mitochondrial fission through modification of the dynamin-related protein Drp1. *Ann N Y Acad Sci* 1201: 34–39

8. Mozdy AD, McCaffery JM, Shaw JM (2000) Dnm1p GTPase-mediated mitochondrial fission is a multi-step process requiring the novel integral membrane component Fis1p. *J Cell Biol* 151: 367–380

9. Tieu Q, Nunnari J (2000) Mdv1p is a WD repeat protein that interacts with the dynamin-related GTPase, Dnm1p, to trigger mitochondrial division. *J Cell Biol* 151: 353–366

10. Otera H, Wang C, Cleland MM, Setoguchi K, Yokota S, Youle RJ, Mihara K (2010) Mff is an essential factor for mitochondrial recruitment of Drp1 during mitochondrial fission in mammalian cells. *J Cell Biol* 191: 1141–1158

11. Loson OC, Song Z, Chen H, Chan DC (2013) Fis1, Mff, MiD49, and MiD51 mediate Drp1 recruitment in mitochondrial fission. *Mol Biol Cell* 24: 659–667

12. Koirala S, Guo Q, Kalia R, Bui HT, Eckert DM, Frost A, Shaw JM (2013) Interchangeable adaptors regulate mitochondrial dynamin assembly for membrane scission. *Proc Natl Acad Sci USA* 110: E1342–E1351

13. Gandre-Babbe S, van der Bliek AM (2008) The novel tail-anchored membrane protein Mff controls mitochondrial and peroxisomal fission in mammalian cells. *Mol Biol Cell* 19: 2402–2412

14. Palmer CS, Osellame LD, Laine D, Koutsopoulos OS, Frazier AE, Ryan MT (2011) MiD49 and MiD51, new components of the mitochondrial fission machinery. *EMBO Rep* 12: 565–573

15. Korobova F, Ramabhadran V, Higgs HN (2013) An actin-dependent step in mitochondrial fission mediated by the ER-associated formin INF2. *Science* 339: 464–467

16. Manor U, Bartholomew S, Golani G, Christenson E, Kozlov M, Higgs H, Spudich J, Lippincott-Schwartz J (2015) A mitochondria-anchored isoform of the actin-nucleating spire protein regulates mitochondrial division. *Elife* 4: e08828

17. Li S, Xu S, Roelofs BA, Boyman L, Lederer WJ, Sesaki H, Karbowski M (2015) Transient assembly of F-actin on the outer mitochondrial membrane contributes to mitochondrial fission. *J Cell Biol* 208: 109–123

18. Korobova F, Gauvin TJ, Higgs HN (2014) A role for myosin II in mammalian mitochondrial fission. *Current Biol* 24: 409–414

19. Joo E, Surka MC, Trimble WS (2007) Mammalian SEPT2 is required for scaffolding nonmuscle myosin II and its kinases. *Dev Cell* 13: 677–690

20. Fung KY, Dai L, Trimble WS (2014) Cell and molecular biology of septins. *Int Rev Cell Mol Biol* 310: 289–339

21. Mostowy S, Cossart P (2012) Septins: the fourth component of the cytoskeleton. *Nat Rev Mol Cell Biol* 13: 183–194

22. Longtine MS, DeMarini DJ, Valencik ML, Al-Awar OS, Fares H, De Virgilio C, Pringle JR (1996) The septins: roles in cytokinesis and other processes. *Curr Opin Cell Biol* 8: 106–119

23. Faty M, Fink M, Barral Y (2002) Septins: a ring to part mother and daughter. *Curr Genet* 41: 123–131

24. Kinoshita M, Noda M (2001) Roles of septins in the mammalian cytokinesis machinery. *Cell Struct Funct* 26: 667–670

25. Hu Q, Milenkovic L, Jin H, Scott MP, Nachury MV, Spiliotis ET, Nelson WJ (2010) A septin diffusion barrier at the base of the primary cilium maintains ciliary membrane protein distribution. *Science* 329: 436–439

26. Kim SK, Shindo A, Park TJ, Oh EC, Ghosh S, Gray RS, Lewis RA, Johnson CA, Attie-Bittach T, Katsanis N *et al* (2010) Planar cell polarity acts through septins to control collective cell movement and ciliogenesis. *Science* 329: 1337–1340

27. Finger FP, Kopish KR, White JG (2003) A role for septins in cellular and axonal migration in *C. elegans*. *Dev Biol* 261: 220–234

28. Huang YW, Yan M, Collins RF, Diciccio JE, Grinstein S, Trimble WS (2008) Mammalian septins are required for phagosome formation. *Mol Biol Cell* 19: 1717–1726

29. Mostowy S, Bonazzi M, Hamon MA, Tham TN, Mallet A, Lelek M, Gouin E, Demangel C, Brosch R, Zimmer C *et al* (2010) Entrapment of intracytosolic bacteria by septin cage-like structures. *Cell Host Microbe* 8: 433–444

30. Dobbelaere J, Barral Y (2004) Spatial coordination of cytokinetic events by compartmentalization of the cell cortex. *Science* 305: 393–396

31. Takizawa PA, DeRisi JL, Wilhelm JE, Vale RD (2000) Plasma membrane compartmentalization in yeast by messenger RNA transport and a septin diffusion barrier. *Science* 290: 341–344

32. Chao JT, Wong AK, Tavassoli S, Young BP, Chruscicki A, Fang NN, Howe LJ, Mayor T, Foster LJ, Loewen CJ (2014) Polarization of the endoplasmic reticulum by ER-septin tethering. *Cell* 158: 620–632

33. Kinoshita M, Field CM, Coughlin ML, Straight AF, Mitchison TJ (2002) Self- and actin-templated assembly of Mammalian septins. *Dev Cell* 3: 791–802

34. Wloga D, Strzyzewska-Jowko I, Gaertig J, Jerka-Dziadosz M (2008) Septins stabilize mitochondria in *Tetrahymena thermophila*. *Eukaryot Cell* 7: 1373–1386

35. Kissel H, Georgescu MM, Larisch S, Manova K, Hunnicutt GR, Steller H (2005) The Sept4 septin locus is required for sperm terminal differentiation in mice. *Dev Cell* 8: 353−364

36. Takahashi S, Inatome R, Yamamura H, Yanagi S (2003) Isolation and expression of a novel mitochondrial septin that interacts with CRMP/CRAM in the developing neurones. *Genes Cells* 8: 81−93

37. Larisch S, Yi Y, Lotan R, Kerner H, Eimerl S, Tony Parks W, Gottfried Y, Birkey Reffey S, de Caestecker MP, Danielpour D *et al* (2000) A novel mitochondrial septin-like protein, ARTS, mediates apoptosis dependent on its P-loop motif. *Nat Cell Biol* 2: 915−921

38. Estey MP, Di Ciano-Oliveira C, Froese CD, Bejide MT, Trimble WS (2010) Distinct roles of septins in cytokinesis: SEPT9 mediates midbody abscission. *J Cell Biol* 191: 741−749

39. Menon MB, Sawada A, Chaturvedi A, Mishra P, Schuster-Gossler K, Galla M, Schambach A, Gossler A, Forster R, Heuser M *et al* (2014) Genetic deletion of SEPT7 reveals a cell type-specific role of septins in microtubule destabilization for the completion of cytokinesis. *PLoS Genet* 10: e1004558

40. Smirnova E, Shurland DL, Ryazantsev SN, van der Bliek AM (1998) A human dynamin-related protein controls the distribution of mitochondria. *J Cell Biol* 143: 351−358

41. Schrader M, Costello JL, Godinho LF, Azadi AS, Islinger M (2015) Proliferation and fission of peroxisomes − an update. *Biochim Biophys Acta* 1863: 971−983

42. Karbowski M, Arnoult D, Chen H, Chan DC, Smith CL, Youle RJ (2004) Quantitation of mitochondrial dynamics by photolabeling of individual organelles shows that mitochondrial fusion is blocked during the Bax activation phase of apoptosis. *J Cell Biol* 164: 493−499

43. De Vos KJ, Allan VJ, Grierson AJ, Sheetz MP (2005) Mitochondrial function and actin regulate dynamin-related protein 1-dependent mitochondrial fission. *Curr Biol* 15: 678−683

44. Ishihara N, Mihara K (2005) Mitochondrial dynamics regulated by fusion and fission. *Tanpakushitsu Kakusan Koso* 50: 931−939

45. Ishihara N, Nomura M, Jofuku A, Kato H, Suzuki SO, Masuda K, Otera H, Nakanishi Y, Nonaka I, Goto Y *et al* (2009) Mitochondrial fission factor Drp1 is essential for embryonic development and synapse formation in mice. *Nat Cell Biol* 11: 958−966

46. Legros F, Lombes A, Frachon P, Rojo M (2002) Mitochondrial fusion in human cells is efficient, requires the inner membrane potential, and is mediated by mitofusins. *Mol Biol Cell* 13: 4343−4354

47. Malka F, Guillery O, Cifuentes-Diaz C, Guillou E, Belenguer P, Lombes A, Rojo M (2005) Separate fusion of outer and inner mitochondrial membranes. *EMBO Rep* 6: 853−859

48. Stavru F, Palmer AE, Wang C, Youle RJ, Cossart P (2013) Atypical mitochondrial fission upon bacterial infection. *Proc Natl Acad Sci USA* 110: 16003−16008

49. Ishihara N, Jofuku A, Eura Y, Mihara K (2003) Regulation of mitochondrial morphology by membrane potential, and DRP1-dependent division and FZO1-dependent fusion reaction in mammalian cells. *Biochem Biophys Res Commun* 301: 891−898

50. Caron J, Fallet C, Tinevez JY, Moisan L, Braitbart LP, Sirat GY, Shorte SL (2014) Conical diffraction illumination opens the way for low phototoxicity super-resolution imaging. *Cell Adh Migr* 8: 430−439

51. Cassidy-Stone A, Chipuk JE, Ingerman E, Song C, Yoo C, Kuwana T, Kurth MJ, Shaw JT, Hinshaw JE, Green DR *et al* (2008) Chemical inhibition of the mitochondrial division dynamin reveals its role in Bax/Bak-dependent mitochondrial outer membrane permeabilization. *Dev Cell* 14: 193−204

52. Sellers JR (1999) Unphosphorylated crossbridges and latch: smooth muscle regulation revisited. *J Muscle Res Cell Motil* 20: 347−349

53. Rolland SG, Lu Y, David CN, Conradt B (2009) The BCL-2-like protein CED-9 of *C. elegans* promotes FZO-1/Mfn1,2- and EAT-3/Opa1-dependent mitochondrial fusion. *J Cell Biol* 186: 525−540

54. Ackema KB, Hench J, Bockler S, Wang SC, Sauder U, Mergentaler H, Westermann B, Bard F, Frank S, Spang A (2014) The small GTPase Arf1 modulates mitochondrial morphology and function. *EMBO J* 33: 2659−2675

55. Labrousse AM, Zappaterra MD, Rube DA, van der Bliek AM (1999) *C. elegans* dynamin-related protein DRP-1 controls severing of the mitochondrial outer membrane. *Mol Cell* 4: 815−826

56. Breckenridge DG, Kang BH, Kokel D, Mitani S, Staehelin LA, Xue D (2008) *Caenorhabditis elegans* drp-1 and fis-2 regulate distinct cell-death execution pathways downstream of ced-3 and independent of ced-9. *Mol Cell* 31: 586−597

57. Ji WK, Hatch AL, Merrill RA, Strack S, Higgs HN (2015) Actin filaments target the oligomeric maturation of the dynamin GTPase Drp1 to mitochondrial fission sites. *Elife* 4: e11553

58. Karbowski M, Spodnik JH, Teranishi M, Wozniak M, Nishizawa Y, Usukura J, Wakabayashi T (2001) Opposite effects of microtubule-stabilizing and microtubule-destabilizing drugs on biogenesis of mitochondria in mammalian cells. *J Cell Sci* 114: 281−291

59. Kim MS, Froese CD, Estey MP, Trimble WS (2011) SEPT9 occupies the terminal positions in septin octamers and mediates polymerization-dependent functions in abscission. *J Cell Biol* 195: 815−826

60. Maimaitiyiming M, Kobayashi Y, Kumanogoh H, Nakamura S, Morita M, Maekawa S (2013) Identification of dynamin as a septin-binding protein. *Neurosci Lett* 534: 322−326

61. Vrabioiu AM, Gerber SA, Gygi SP, Field CM, Mitchison TJ (2004) The majority of the *Saccharomyces cerevisiae* septin complexes do not exchange guanine nucleotides. *J Biol Chem* 279: 3111−3118

62. Farkasovsky M, Herter P, Voss B, Wittinghofer A (2005) Nucleotide binding and filament assembly of recombinant yeast septin complexes. *Biol Chem* 386: 643−656

63. Sirajuddin M, Farkasovsky M, Zent E, Wittinghofer A (2009) GTP-induced conformational changes in septins and implications for function. *Proc Natl Acad Sci USA* 106: 16592−16597

64. Soubannier V, McLelland GL, Zunino R, Braschi E, Rippstein P, Fon EA, McBride HM (2012) A vesicular transport pathway shuttles cargo from mitochondria to lysosomes. *Curr Biol* 22: 135−141

65. Mozdy AD, McCaffery JM, Shaw JM (2000) Dnm1p GTPase-mediated mitochondrial fission is a multi-step process requiring the novel integral membrane component Fis1p. *J Cell Biol* 151: 367−380

66. Tieu Q, Nunnari J (2000) Mdv1p is a WD repeat protein that interacts with the dynamin-related GTPase, Dnm1p, to trigger mitochondrial division. *J Cell Biol* 151: 353−366

67. Friedman JR, Lackner LL, West M, DiBenedetto JR, Nunnari J, Voeltz GK (2011) ER tubules mark sites of mitochondrial division. *Science* 334: 358−362

68. Shibata Y, Voss C, Rist JM, Hu J, Rapoport TA, Prinz WA, Voeltz GK (2008) The reticulon and DP1/Yop1p proteins form immobile oligomers in the tubular endoplasmic reticulum. *J Biol Chem* 283: 18892−18904

69. Spiliotis ET, Kinoshita M, Nelson WJ (2005) A mitotic septin scaffold required for Mammalian chromosome congression and segregation. *Science* 307: 1781−1785

70. Yoon Y, Pitts KR, McNiven MA (2001) Mammalian dynamin-like protein DLP1 tubulates membranes. *Mol Biol Cell* 12: 2894−2905

71. Frezza C, Cipolat S, Scorrano L (2007) Organelle isolation: functional mitochondria from mouse liver, muscle and cultured fibroblasts. *Nat Protoc* 2: 287 – 295

72. Stavru F, Bouillaud F, Sartori A, Ricquier D, Cossart P (2011) *Listeria monocytogenes* transiently alters mitochondrial dynamics during infection. *Proc Natl Acad Sci USA* 108: 3612 – 3617

73. de Chaumont F, Dallongeville S, Chenouard N, Herve N, Pop S, Provoost T, Meas-Yedid V, Pankajakshan P, Lecomte T, Le Montagner Y *et al* (2012) Icy: an open bioimage informatics platform for extended reproducible research. *Nat Methods* 9: 690 – 696

74. De Vos KJ, Sheetz MP (2007) Visualization and quantification of mitochondrial dynamics in living animal cells. *Methods Cell Biol* 80: 627 – 682

75. Lagache T, Sauvonnet N, Danglot L, Olivo-Marin JC (2015) Statistical analysis of molecule colocalization in bioimaging. *Cytometry A* 87: 568 – 579

76. Brenner S (1974) The genetics of *Caenorhabditis elegans*. *Genetics* 77: 71 – 94

77. Kamath RS, Ahringer J (2003) Genome-wide RNAi screening in *Caenorhabditis elegans*. *Methods* 30: 313 – 321

78. Rual JF, Ceron J, Koreth J, Hao T, Nicot AS, Hirozane-Kishikawa T, Vandenhaute J, Orkin SH, Hill DE, van den Heuvel S *et al* (2004) Toward improving *Caenorhabditis elegans* phenome mapping with an ORFeome-based RNAi library. *Genome Res* 14: 2162 – 2168